Potential-Induced Ordering Transition of the Adsorbed Layer at the Ionic Liquid/Electrified Metal Interface

Sami Tazi, Mathieu Salanne,* Christian Simon, and Pierre Turq

UPMC Universite Paris 06, CNRS, ESPCI, UMR 7195, PECSA, F-75005, Paris, France

Michael Pounds

School of Chemistry, University of Edinburgh, Edinburgh EH9 3JJ, U.K.

Paul A. Madden

Department of Materials, University of Oxford, Parks Road, Oxford OX1 3PH, U.K.

Received: April 5, 2010; Revised Manuscript Received: May 17, 2010

The potential-driven ordering transition of a LiCl layer adsorbed on the (100) surface of a metallic aluminum electrode is studied by molecular dynamics simulations. The transition causes a sharp peak in the potential dependence of the differential capacitance of the interface. This result is in qualitative agreement with recently reported experimental work on the interface between a room temperature ionic liquid and a well-defined Au(100) surface. In the LiCl/Al simulations, the transition occurs when the interaction model includes the induction of dipoles on the ions of the liquid by their mutual interaction and their interaction with the electrode surface as well as the polarization of the metal by the charges and dipoles on the ions ("image" interactions). When the electrode or ion polarization effects are not included, the transition is no longer observed. The interaction between the induced charges on the metal atoms and the induced dipoles on the ions creates an additional screening, which stabilizes the formation of a crystalline layer at the anode. When the crystallographic plane of the metal is changed to (110) instead of (100), the two first adsorbed layer are crystalline on both the anode and the cathode, but the structure is different: the crystal is formed through an epitaxial mechanism to adapt to the electrode surface structure. In the case of the (110) crystallographic plane, the charging of the adsorbed layer occurs through the formation of nonstoichiometric crystalline layers.

I. Introduction

Spurred by possible technological applications, the pure ionic liquid/electrified metal interface has received an increasing amount of attention in recent years. High temperature molten salts are potential solvents for the pyroprocessing of nuclear waste[1−6] or the electrochemical deposition of refractory metals.[7,8] Room temperature ionic liquids (RTILs), are used as electrolytes in electrochemical supercapacitors,[9−11] batteries, and fuel cells.[12] In all these applications, a better understanding of the properties of the ionic liquid in the vicinity of the charged surface would be beneficial.

Unlike dilute electrolyte solutions, whose interfaces with metals are well described by the double-layer description provided by the Gouy−Chapman−Stern (GCS) theory, no theoretical model has yet emerged for the study of ionic liquids. The GCS theory, which should be valid for electrolytes of moderate concentration only, has therefore often be used for the interpretation of data on molten salts/metal interfaces.[13] The most important effort for improving this situation is the work of Kornyshev.[14] On the basis of a Poisson−Boltzmann lattice-gas model and accounting for the finite size of the ions, this author derived an analytical formula for the potential dependence of the differential capacitance (DC). A spectacular result provided by this theory (the mean field theory, MFT) is the possibility of observing a maximum of the DC close to the point of zero charge, whereas the GCS analysis gives a U-shaped dependence for the DC in this region. However, as pointed out by Kornyshev himself, the MFT remains somewhat limited, mainly because the ion-correlation effects are not taken into account: in pure ionic liquids, these effects are very strong and lead to important charge-density oscillations close to the interface. This has been confirmed by molecular dynamics (MD) simulations of molten salts[15−18] and of RTILs, modeled either explicitly[19,20] or using model systems consisting of charged spheres,[21,22] eventually supplemented by a neutral tail.[23] In all cases, the cation and anion density profiles show oscillations, revealing the existence of *overscreening* effects in these media. Nevertheless, in some of these studies,[21,22] a maximum was observed at the PZC for the capacitance, in agreement with the MFT. Such so-called "bell-shaped" DCs (as opposed to the "U-shaped" DCs obtained in dilute aqueous electrolytes, in agreement with GCS theory) have also been obtained in some experimental work,[24,25] which seemed to appear as a corroboration of the MFT model. The situation is, in fact, much less clear, since most of the experiments provide nontrivially shaped DCs.[26−30] Moreover, Lockett et al. showed the existence of important hysteresis effects[31] in the capacitance curve, which were confirmed and analyzed in a recent study of the interface between an ionic liquid and a platinum electrode.[32]

In previous work, we presented a method for parametrizing a model of the interactions between the ions in an ionic liquid (LiCl) and a metallic (aluminum) surface.[17] The interaction model includes the induction of dipoles on the ions of the liquid by their mutual interaction and the interaction with the electrode

* Corresponding author. E-mail: mathieu.salanne@upmc.fr.

10.1021/jp1030448
Published on Web 06/09/2010

surface as well as the polarization of the metal by the ionic charges and dipoles ("image" interactions). The electrolyte layer close to the interface was found to exhibit a potential-driven structural transition, which leads to a maximum in the differential capacitance as a function of applied potential. This was the first simulation of an ionic liquid/metal interface in which such a transition was observed, but experimental evidence for similar phenomena has already been reported by several groups.[25,33−35] Here, we study the influence of two key physical parameters on this observation. First, we demonstrate the influence of ion polarization effects on the formation of an ordered adsorbed layer of electrolyte at the surface of the metal. Second, we show the importance of the structure of the metal surface itself by changing the crystallographic plane of aluminum facing the LiCl electrolyte.

II. Model and Methods

A. Interaction Potential. The coulomb and polarization interactions involving the N ions of the melt and the M atoms of the electrode slabs are represented by the potential,

$$U_{\mathrm{tot}} = U_{\mathrm{c}}(\{\mathbf{r}_i\}_{i=1,N}, \{q_j\}_{j=1,M}) + U_{\mathrm{vdW}}(\{\mathbf{r}_i\}_{i=1,N}) + U_{\mathrm{pol}}(\{\mathbf{r}_i\}_{i=1,N}, \{\boldsymbol{\mu}_i\}_{i=1,N}, \{q_j\}_{j=1,M}) + U_{\mathrm{constraint}}(\{q_j\}_{j=1,M}) \quad (1)$$

where the first term is the total Coulomb energy of the system,

$$U_{\mathrm{c}} = \frac{1}{2}\int\int \frac{\rho(\mathbf{r}')\,\rho(\mathbf{r}'')\,\mathrm{d}\mathbf{r}'\,\mathrm{d}\mathbf{r}''}{|\mathbf{r}' - \mathbf{r}''|} \quad (2)$$

for a distribution of metallic and ionic charges $\rho = \sum_{j=1}^{\mathrm{M}} \rho_j + \sum_{i=1}^{\mathrm{N}} \rho_i$, which have, respectively, a diffuse (Gaussian) and a discrete (point charge) character:

$$\rho_j(\mathbf{r}) = q_j A \exp\left(-|\mathbf{r} - \mathbf{r}_j|^2 \eta^2\right) \quad (3)$$

$$\rho_i(\mathbf{r}) = z_i\, \delta(\mathbf{r} - \mathbf{r}_i) \quad (4)$$

where $A = \eta^3\pi^{3/2}$ is a normalization constant, η being the width of the Gaussian distribution. In our application, the full system consists of two infinite parallel planar electrodes enclosing a set of melt ions. The Coulomb energy is expressed through a two-dimensional Ewald summation, as described in ref 16. Note that this expression will contain a self-energy for the interaction of each Gaussian charge density with itself (any self-energy of the point charges is a trivial constant). The potential experienced by any charge is obtained from the partial derivative of this expression with respect to that charge

$$V_j = \left[\frac{\partial U_{\mathrm{c}}}{\partial q_j}\right]_{q_i, i\neq j} \quad (5)$$

The model for the metallic electrodes is derived from the work of Siepmann and Sprik,[36] in which the value of the charge on each electrode atom at each time step in a MD procedure is obtained by requiring that the potential experienced by each charge j in that electrode be a constant, V_j^0, which is the value of the preset electrode potential and will take the same value for all ions in a particular electrode. The potential within the electrode is thus a constant, which is the electrostatic condition on the potential inside a conductor. This condition is achieved by adding a constraint term,

$$U_{\mathrm{constraint}} = -\sum_{j=1}^{M} V_j^0 q_j \quad (6)$$

and by minimizing the total potential energy with respect to all the variable charges simultaneously, which ensures the constant potential condition is fulfilled.

The van der Waals interactions consist of a repulsion due to the overlap of the ionic electron densities between themselves and with the valence electrons of the metal and an attractive dispersion term. We chose to model these effects with a simple pair potential,

$$U_{\mathrm{vdW}} = \sum_{i<j}^{N+M}\left(B^{ij}\exp\left(-a^{ij}r_{ij}\right) - \sum_{n=6,8}\frac{C_n^{ij} f_n^{ij}(r_{ij})}{r_{ij}^n}\right) \quad (7)$$

where the f_n^{ij} ($n = 6, 8$) functions are Tang−Toennies damping functions that contain a single parameter, the (inverse) range b_n^{ij} at which the asymptotic forms of the dispersion terms are suppressed.[37]

Finally, the ion polarization term includes charge-dipole and dipole−dipole terms:

$$\begin{aligned} U_{\mathrm{pol}} &= \sum_{i,j\neq i}^{N}(1 - c^{ij} f_4^{ij}(r_{ij}))\,\boldsymbol{\mu}_i\cdot\mathbf{T}_{ij}^1 z_j \\ &- \sum_{i,j\neq i}^{N}(1 - c^{ji} f_4^{ij}(r_{ij}))\,\boldsymbol{\mu}_j\cdot\mathbf{T}_{ij}^1 z_i \\ &+ \sum_{i=1}^{N}\sum_{j=1}^{M}\boldsymbol{\mu}_i\cdot\mathbf{T}_{ij}^1 q_j + \mathbf{F}_{ij}^{sr}\cdot\boldsymbol{\mu}_i \\ &- \sum_{i,j\neq i}^{N}\boldsymbol{\mu}_i\mathbf{T}_{ij}^2\boldsymbol{\mu}_j + \sum_{i=1}^{N}\frac{1}{2\alpha_i}|\boldsymbol{\mu}_i|^2 \end{aligned} \quad (8)$$

where all the terms except the third one are the usual terms that appear within the polarizable ion model:[38] α_i is the ionic polarizability of the ion i and $\mathbf{T}_{ij}^n$ are the normal charge-dipole ($n = 1$) and dipole−dipole ($n = 2$) interaction tensors, to be evaluated in 2D periodic boundary conditions by the Ewald method.[39] The c^{ij} parameters arise from the charge damping of the dipoles, which again involves the use of Tang−Toennies functions (with $n = 4$). The interaction between the electrode and the ionic melt consists of charge-dipole interactions, supplemented by a short-range contribution to the induction of dipoles on the melt ions, which is represented by the function

$$\mathbf{F}_{ij}^{\mathrm{sr}}(\mathbf{r}_{ij}) = \hat{\mathbf{r}}_{ij}A^{ij}\exp\left(-\beta^{ij}(r_{ij} - d^{ij})^2\right) \quad (9)$$

where $\hat{\mathbf{r}}_{ij}$ is a unit vector. $\mathbf{F}^{sr}$ is therefore directed along the interatomic separation. It behaves like an electric field, which distorts the charge cloud of a melt ion due to overlap-mediated interactions with the electrode atoms.[17] The set of parameters used in the present study are given in Table 1. They were obtained from a dipole-and-force-fitting procedure involving first-principles density functional theory calculations.[17]

B. Simulation Details. Several MD simulations of the Al electrode−LiCl melt have been performed for different values

TABLE 1: The Fitted Parameters for Interaction Potential[a,b]

	a	B	C_6	C_8	b_6	b_8
Cl−Cl	1.5917	115.1	144.9	100.013	1.6835	1.6468
Cl−Li	1.9169	54.8	0.001	0.001	1.4922	9.2454
Cl−Al	2.7831	29542.0	226.110	779.563	2.4847	2.5010
Li−Li	5.8543	47.5	0.001	0.001	6.4376	1.7060
Li−Al	3.3244	72874.9	0.420	3.407	9.6913	7.1163

[a] One set only is provided for the polarization term parameters because the Li^+ ions are considered to be nonpolarizable.[40] All values are in atomic units. [b] $A = 1.22134 \times 10^{-2}$; $\beta = 3.33853 \times 10^{-1}$; $d = 3.68818$; $\alpha_{Cl^-} = 20.0$; $b_4 = 1.861$; $c = 2.079$.

of the applied electrode potential difference to examine the potential dependence of the melt structure at the interface. Two different crystallographic planes were studied. In the first case, the electrodes included 432 *fixed* Al atoms arranged in an fcc structure with the (100) surface exposed to the melt. The dimensions of the cell were 24.297 Å in the x and y directions and 49.8345 Å between the innermost layer of electrode atoms along z. This box was used for two series of simulations, differing by the inclusion/absence of polarization effects for the chloride anions, all the other parameters of the interaction potential being kept the same.

In the second case, the electrodes included 288 *fixed* Al atoms arranged in an fcc structure with the (110) surface exposed to the melt. The dimensions of the cell were 24.295 Å and 22.908 Å in the x and y directions, respectively, and 50.456 Å between the innermost layer of electrode atoms along z. In both setups, the melt region included 500 Li^+ and 500 Cl^- ions, and the x and y distances were chosen to match the corresponding number of fcc Al unit cells. The simulations were initiated by taking a melt configuration from a bulk liquid LiCl simulation in which the cell dimensions had been matched to these values. A rendering of a representative configuration of the system is shown in Figure 1. The simulation was then run for 100 ps to allow for equilibration and this was followed by 75 ps of production runs in the NVT statistical ensemble.

The simulations with different applied potentials were initiated in sequence, and an equilibration period of 60 ps was allowed before collecting statistics. The applied potential differences $|V^+ - V^-|$ investigated ranged from 0.0 to 5.0 V. One should note that even if the system is physically realistic, because the interaction potentials have been parametrized from first-principles calculations,[17] it does not correspond to a real system: (1) the melting of aluminum occurs before the one of LiCl, and (2) such important potential differences cannot be reached in electrochemistry experiments. It is nevertheless a first step toward the study of the eutectic LiCl−KCl//Al interface, which is relevant to pyroprocessing of nuclear waste.[1−4]

III. Results and Discussion

A. Ion Polarization Effects on the Adsorbed Layer Structure. Most MD studies involving an ionic liquid/electrified metal interface have employed a somewhat simplified model, in which (1) the metallic walls carry constant charges, and (2) ion polarization effects are not taken into account.[15,19−22] In that case, the electrostatic potential at different atoms within each electrode is not controlled during the simulations, and the interaction between the melt and the metal is not completely captured: in a real system, the electronic charge distribution of the metal is allowed to fluctuate to adapt to the adjacent melt structure. No phase transition of the adsorbed layer was reported from such simulations, in contrast to our previous work,[17] although ordering effects were observed by Kislenko et al. in their study of the interface between a RTIL and a model graphite surface.[42] It is therefore of interest to determine which of the two effects, that is, the ions or the electrode polarization, is paramount for seeing this effect. A simulation study of the interface between LiCl and a planar metallic electrode accounting for the polarization of the electrode, but not of the ions, was recently reported,[18] and again, no phase transition was observed. We have therefore chosen to study directly the effect of chloride anion polarization in the present work.

The ionic density profiles across the simulation cell, as obtained without and with the inclusion of ion polarization effects, are plotted on Figures 2 and 3 for different values of the applied potential difference. In both cases, strong oscillations are observed; the Li^+ ion density oscillations are out-of-phase as compared to the Cl^- ones. The application of the potential increases the amplitude of these oscillations. They are due to the overscreening effect: the first adsorbed layer delivers a much larger counterion charge than required to neutralize the charge on the electrode. The second layer overcompensates it by a charge of the opposite sign, and these oscillations extend, decaying, over several layers into the bulk. Similar overscreening régimes have been reported in all the previous MD simulation studies.[15−22] Such ionic density profiles are not expected in the GCS theory, which is to be expected, since it was developed for aqueous electrolyte at moderate salt concentration and builds upon simplifying assumptions that are far from being fulfilled in our system. They are also not predicted by the MFT of Kornyshev, which was anticipated by this author.[14] There is, therefore, a need for the development of more complex theories encompassing the ion−ion correlation effects; in the absence of such a theory, MD simulations should provide the best background for interpreting experimental observations.

An important difference is observed when the ion polarization effects are included in the simulation model, with the appearance of a strongly adsorbed layer of both Li^+ and Cl^- ions at the anode. When viewed from the direction perpendicular to the interface, as shown in Figure 4, the ion positions in the absorbed layer are seen to have a crystalline ordering, which appears to be commensurate with the underlying Al lattice. The distance between the atoms of the electrode and the ions in the first absorbed layer is also reduced by the inclusion of the polarization effects.

The crystallized layer appears near the point of zero charge (PZC) when the electrode becomes positively charged. It forms through an epitaxial mechanism, with the ions facing the hollow site between aluminum atoms. The fact that it appears only upon inclusion of polarization means that an additional screening effect is involved. This is depicted in Figure 5 which shows the dipole distribution for the ions in the adsorbed layer. Whatever the applied potential, this distribution remains unchanged and centered around 0 D for the x and y components, showing that no particular orientation of the dipole occurs in the plane parallel to the surface.

In contrast, the z-component of the dipole is directed toward the melt: this corresponds to an additional negative charge between the liquid and the electrode, which contributes to the screening of the electrode charge. The magnitude of this dipole increases with the electrode potential. For small applied potentials, its value is comparable to the one observed for a Cl^- anion in the solvation shell of a La^{3+} ions in aqueous solutions.[43] But at higher potentials, the size of the dipole may be somewhat unphysical. We recall that such large applied potentials cannot be reached experimentally: the oxidation of

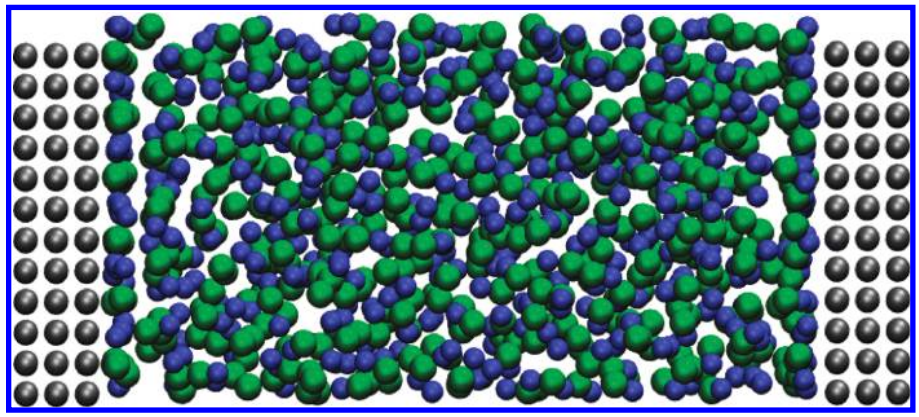

Figure 1. A rendering of a representative configuration of the system studied. The crystallographic plane facing the melt is the (100), and the ion polarization effects are included. The positive electrode is located at the left end of the simulation cell ($V^+ = -V^- = 1$ V so that the applied potential difference is $\Delta V = 2$ V). The Cl^-, Li^+, and Al atoms are green, blue, and black, respectively. Snapshot obtained with the VMD program.[41]

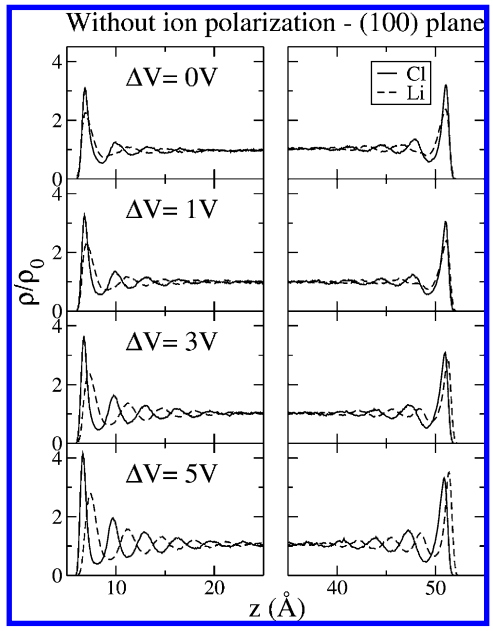

Figure 2. Ionic density profiles across the simulation cell for different values of the applied potential difference, without taking into account the polarization of the ions. The electrode set at a positive potential V^+ is located at the left end of the simulation cell. ρ_0 is the bulk melt density.

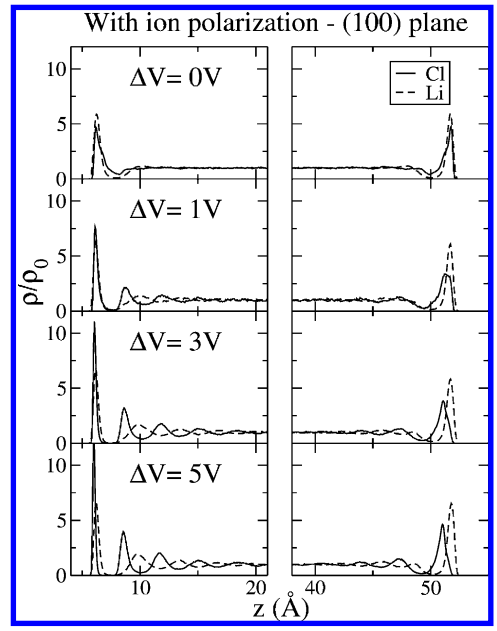

Figure 3. Ionic density profiles across the simulation cell for different values of the applied potential, taking into account the polarization of the ions. The electrode set at a positive potential V^+ is located at the left end of the simulation cell. ρ_0 is the bulk melt density.

Cl^- into Cl_2 would occur. The additional screening induced by the dipoles is also responsible for the diminution of the approach distance between the electrode and the liquid.

So far, three experimental studies using in situ scanning tunnel microscopy (STM) have provided direct evidence of similar potential-induced structural transitions in the absorbed layer in ionic liquids. In the first case, a disorder−order phase transition was observed in the adsorbed PF_6^- layer at the electrified ionic liquid/Au (111) interface. The structural change is gradual, and it ends up as a $(\sqrt{3} \times \sqrt{3})$ phase.[33] The same authors reported a transformation from a well-ordered $AlCl_4^-$ adlayer to a $(\sqrt{3} \times \sqrt{19})$ superstructure, which was observed during the underpotential deposition of Cd on Au (111) in an acidic chloroaluminate ionic liquid.[34] The last study concerns the interface between imidazolium-based ionic liquids and Au (100). Su et al. showed that the adsorption of 1-butyl-3-methylimidazolium (BMI^+) cations follows a potential-driven disorder−order transition above a given cathodic potential.[25]

Similar ordering effects at Pt surfaces have also been detected in sum-frequency spectroscopy and inferred from electrochemical measurements.[44,45] All these examples concern RTILs and so differ from the system studied here because of the lower temperature and the molecular shape of the ions. Yet, the different nature of the ions that experience the phase transition in these applications (PF_6^- and $AlCl_4^-$ anions, BMI^+ cations) suggests that the phenomenon may occur in a much wider variety of systems. Our approach shows that additional degrees of freedom beyond simply the interactions of charged spheres (in our case, the induced ionic dipole) allow for a more efficient screening of the surface charge and facilitate the structural changes. In RTILs, the internal charge distribution within the molecular ions is very likely to play that important role. In realistic MD simulations of RTILs/electrified metal interfaces, important care should therefore be taken to choose the relevant set of partial charges carried by the atoms,[46] and in some cases, ion polarization effects will also have to be accounted for in the interaction potential.[47,48] On the other hand, simplified models[21−23] will play an important role in decoupling the various mechanisms involved during ionic adsorption on metallic electrodes.

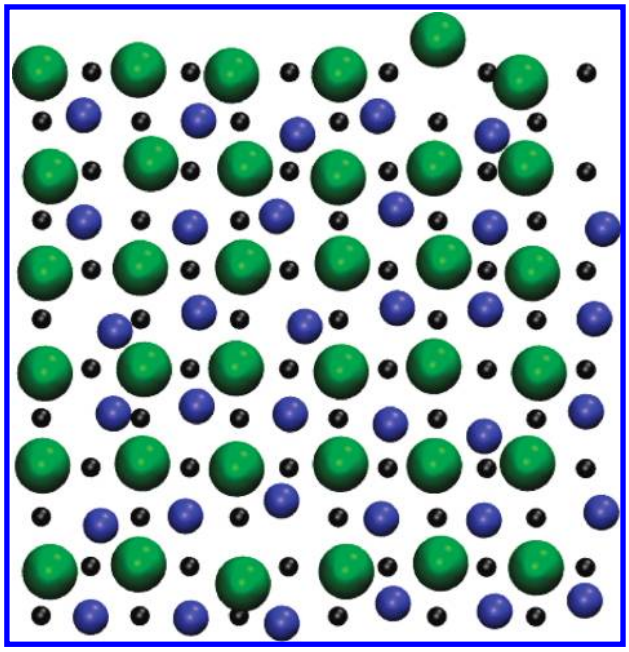

Figure 4. A rendering of a representative configuration of the adsorbed crystalline layer on the anode ($V^+ = 1.0$ V). The crystallographic plane facing the melt is the (100), and the ion polarization effects are included. Only the surface layer of Al atoms is represented. Large green spheres, Cl^- ions; medium blue spheres, Li^+ ions; and small black spheres, Al atoms. Snapshot obtained with the VMD program.[41]

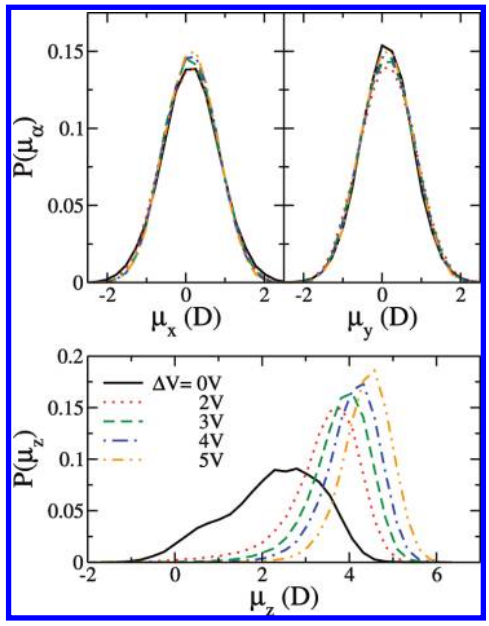

Figure 5. Distribution of the chloride dipole components μ_α in the adsorbed crystalline layer for different values of the applied potential difference (the metal crystallographic plane is the (100), and ion polarization effects are, indeed, taken into account). $\alpha = x$, y are the components parallel to the electrode; $\alpha = z$ is normal to the interface.

B. Changing the Electrode Crystallographic Plane. The epitaxial mechanism involved in the structural transition of the absorbed layer raises the issue of the importance of the metal crystallographic plane facing the melt. The ionic density profiles obtained in the case of a (110) aluminum plane are shown in Figure 6. Again, two different regimes are observed: first, the oscillations associated with overscreening in the innermost layer of the electrolyte (they are more pronounced on the anodic side), and second, two well-resolved adsorption peaks close to the

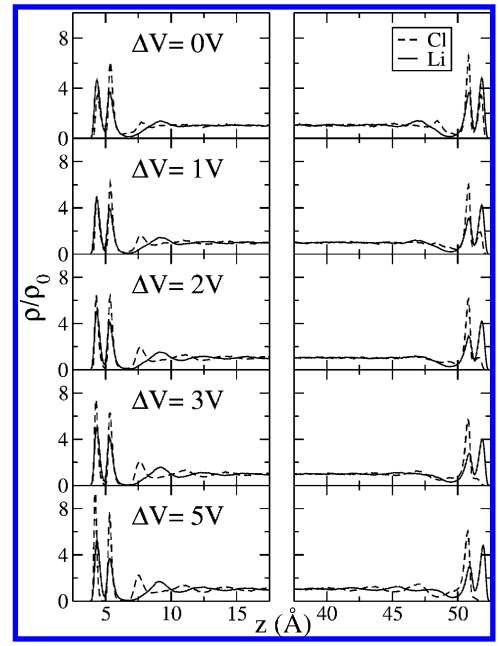

Figure 6. Ionic density profiles across the simulation cell for different values of the applied potential difference for the (110) crystallographic plane. The electrode set at a positive potential V^+ is located at the left end of the simulation cell. ρ_0 is the bulk melt density.

electrode. By computing the in-plane $Cl^- - Cl^-$ structure factor[17] in these layers (not shown here), we obtain very sharp diffraction peaks corresponding to the Al−Al separation in the (110) plane. There are, therefore, two crystalline adsorbed layers in this case. Unlike the (100) surface, these two layers are present whatever the electrode potential, and so no potential-driven phase transition occurs in that system.

The electrolyte polarization mechanism, which screens the electrode charge, at the (110) surface also appears to be different from the (100). Here, we observe different intensities for the adsorption peak of the two ions in their density profiles. The density profile of the Li^+ ions seems to remain unchanged from one applied potential to another and from the anode to the cathode. The Cl^- anions are not present in the first layer when the electrode has a large negative charge, as shown in the bottom-right panel of Figure 6 (in that case, the first adsorbed layer can therefore be viewed as a Stern layer of adsorbed Li^+ ions), and they progressively adsorb when this charge becomes less negative. The crystallized layers therefore have a non stoichiometric character, allowing for a strong polarization of the interface. Such a structure is shown in Figure 7, where it clearly appears that the number of adsorbed Li^+ ions is larger than that of Cl^-.

C. Differential Capacitances. Ionic liquid/electrified metal interfaces are often characterized by their differential capacitances (C_{diff}). From our simulations, this quantity can be extracted by differentiation of the surface charge with respect to the potential difference across the interface:

$$C_{diff} = \frac{\partial \Sigma}{\partial \Delta V'} \tag{10}$$

where Σ is the total charge accumulated on the electrode and $\Delta V'^{\pm} - V^{bulk}$ is the potential difference between the electrode and the bulk liquid and, therefore, differs from the applied potential difference (ΔV) described above. The evolution of the surface charge density ($\sigma = \Sigma/A$, where A is the electrode

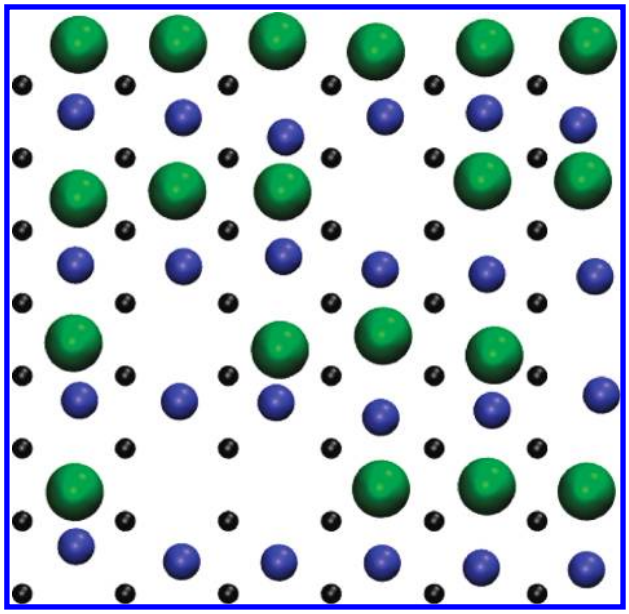

Figure 7. A rendering of a representative configuration of the adsorbed crystalline layer on the anode ($V^+ = 0.0$ V). The crystallographic plane facing the melt is the (110), and the ion polarization effects are included. Only the surface layer of Al atoms is represented. Large green spheres, Cl^- ions; medium blue spheres, Li^+ ions; and small black spheres, Al atoms. Snapshot obtained with the VMD program.[41]

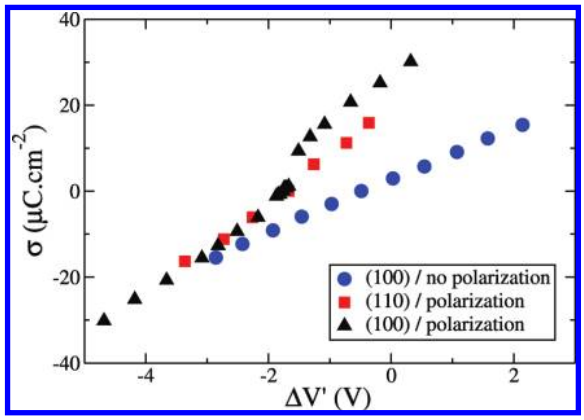

Figure 8. Variation of the surface charge with the potential drop across the interface $\Delta V'^{\pm} - V^{bulk}$. A discontinuity is observed near the PZC for the data corresponding to the (100) plane when ion polarization effects are taken into account.

surface) with increasing $\Delta V'$ is displayed in Figure 8. The dependence is mainly linear, with a discontinuity in the case of the (100) plane with polarization effects. The extracted surface DC values are 10.4 and 10.2 μF cm^{-2} for the two different linear parts of the latter case, 9.9 μF cm^{-2} for the (110) plane and 6.1 μF cm^{-2} for the (100) plane without polarization effects.

From the similarity among all the DCs with polarization effect, we anticipate that the adsorbed layer structure (liquid or solid-like) does not influence greatly the charging of the electrode. On the contrary, when passing from a polarizable ion model to a nonpolarizable one, we expect the dielectric constant to be reduced by (roughly) the square root of the high-frequency dielectric permittivity associated with the polarization of the ions.[49] A typical value for this permittivity is 2, which explains the different values obtained for the DCs. In Figure 8, we also observe an important change in the PZC, which goes toward more negative interfacial potential difference values when polarization effects are included. This again illustrates the additional screening of the electrode charge by the induced dipoles of the Cl^- ions in that case. It could be noted that the PZC values seem large as compared with experimental ones; however, one must remember that the experimental quantity is always measured with respect to a reference electrode, whereas in our simulations, we are dealing with absolute potentials.

The charge density accumulated at the electrode−electrolyte interface is the derivative of the surface tension with respect to the potential difference across the interface:

$$\sigma = -\left(\frac{\partial \gamma}{\partial \Delta V'}\right)_{T,P,n_i} = -\left(\frac{\partial^2 G}{\partial \Delta V' \partial A}\right)_{T,P,n_i} \qquad (11)$$

where G is the Gibbs free energy of the electrolyte. The presence of a discontinuity therefore means that the structural transition observed behaves like a phase transition of second order. It corresponds to a peak in the DC, which may allow us to provide a new interpretation for some experimental observations. Indeed, several experimental studies showed the existence of such peaks in the case of RTILs.[24,25] These were first interpreted with the help of MFT because this theory predicts such a peak under certain conditions.

In our case, the presence of the peak is correlated with the potential-induced phase transition, which is in agreement with the direct experimental observations of Su et al. The induced ionic dipoles are additional degrees of freedom that facilitate the structural change. In the case of RTILs, this role could be played by the molecular shape of the ions, leading, for example, to planar reorientations in the case of imidazolium ions. Sharp transitions at the ionic liquid/electrified metal interface may not always be detected from differential DCs because of the polydispersity and the roughness of the metallic surface facing the bulk liquid, and it is certainly the case that nontrivially shaped DCs have normally been observed experimentally.[26−32]

IV. Conclusion

In this study, we have shown that a structural transition occurs in the LiCl layer adsorbed on a metallic electrode, only under particular conditions. First, the interaction model must include the polarization of both the ions and the metal atoms. The interaction between the metallic charges and the dipoles creates an additional screening, which stabilizes the formation of a crystalline layer at the anode when the metal atoms carry positive charges. When one of these polarization effects is removed, the phase transition is no longer observed, and the adsorbed layer remains liquidlike. Second, when the crystallographic plane of the metal is changed to (110) instead of (100), the two first adsorbed layer are crystalline on both the anode and the cathode, with a different structure. In all cases, the crystal is formed through an epitaxial mechanism to adapt to the electrode surface structure. When the (110) crystallographic plane is facing the melt, the charging of the adsorbed layer occurs through the formation of nonstoichiometric crystalline layers.

Such 2-dimensional phase transitions have already been reported in experimental works concerning interfaces between a room temperature ionic liquid and a well-defined metallic surface.[33−35,25] In one of these studies, the phase transition was linked with the existence of a peak in the differential capacitance.[25] This is also the case in our study, in which we observe a jump in the metallic electrode surface charge variation with respect to the potential drop across the interface.

Acknowledgment. We acknowledge the PCR ANSF and GNR PARIS of the PACEN program (CNRS) for financial

support. Sami Tazi is the beneficiary of a fellowship from UPMC−Fondation pour les Energies de Demain−Institut de France.

References and Notes

(1) Lantelme, F.; Berghoute, Y. *J. Electrochem. Soc.* **1999**, *146*, 4137–4144.
(2) Lantelme, F.; Cartailler, T.; Berghoute, Y.; Hamdani, M. *J. Electrochem. Soc.* **2001**, *148*, C604–C613.
(3) Masset, P.; Bottomley, D.; Konings, R.; Malmbeck, R.; Rodrigues, A.; Serp, J.; Glatz, J.-P. *J. Electrochem. Soc.* **2005**, *152*, A1109–A1115.
(4) Masset, P.; Konings, R.; Malmbeck, R.; Serp, J.; Glatz, J.-P. *J. Nucl. Mater.* **2005**, *344*, 173–179.
(5) Hamel, C.; Chamelot, P.; Laplace, A.; Walle, E.; Dugne, O.; Taxil, P. *Electrochim. Acta* **2007**, *52*, 3995–4003.
(6) Salanne, M.; Simon, C.; Turq, P.; Madden, P. *J. Phys. Chem. B* **2008**, *112*, 1177–1183.
(7) Groult, H.; Barhoun, A.; El Ghallali, H.; Borensztjan, S.; Lantelme, F. *J. Electrochem. Soc.* **2008**, *155*, E19–E25.
(8) El Ghallali, H.; Groult, H.; Barhoun, A.; Draoui, K.; Krulic, D.; Lantelme, F. *Electrochim. Acta* **2009**, *54*, 3152–3160.
(9) Simon, P.; Gogotsi, Y. *Nat. Mater.* **2008**, *7*, 845–854.
(10) Largeot, C.; Portet, C.; Chmiola, J.; Taberna, P.; Gogotsi, Y.; Simon, P. *J. Am. Chem. Soc.* **2008**, *130*, 2730–2731.
(11) Lin, R.; Huang, P.; Segalini, J.; Largeot, C.; Taberna, P.; Chmiola, J.; Gogotsi, Y.; Simon, P. *Electrochim. Acta* **2009**, *54*, 7025–7032.
(12) Armand, M.; Endres, F.; MacFarlane, D.; Ohno, H.; Scrosati, B. *Nat. Mater.* **2009**, *8*, 621–629.
(13) Kisza, A. *J. Electroanal. Chem.* **2002**, *534*, 99–106.
(14) Kornyshev, A. *J. Phys. Chem. B* **2007**, *111*, 5545–5557.
(15) Lanning, O.; Madden, P. *J. Phys. Chem. B* **2004**, *108*, 11069–11072.
(16) Reed, S.; Lanning, O.; Madden, P. *J. Chem. Phys.* **2007**, *126*, 084704.
(17) Pounds, M.; Tazi, S.; Salanne, M.; Madden, P. *J. Phys.: Condens. Matter* **2009**, *21*, 424109.
(18) Vatamanu, J.; Borodin, O.; Smith, G. *Phys. Chem. Chem. Phys.* **2010**, *12*, 170–182.
(19) Pinilla, C.; Popolo, M. D.; Kohanoff, J.; Lynden-Bell, R. *J. Phys. Chem. B* **2007**, *111*, 4877–4884.
(20) Feng, G.; Zhang, J.; Qiao, R. *J. Phys. Chem. C* **2009**, *113*, 4549–1559.
(21) Fedorov, M.; Kornyshev, A. *J. Phys. Chem. B* **2008**, *112*, 11868–11872.
(22) Fedorov, M.; Kornyshev, A. *Electrochim. Acta* **2008**, *53*, 6835–6840.
(23) Fedorov, M.; Georgi, N.; Kornyshev, A. *Electrochem. Commun.* **2010**, *12*, 296–299.
(24) Islam, M.; Alam, M.; Ohsaka, T. *J. Phys. Chem. C* **2008**, *112*, 16568–16574.
(25) Su, Y.-Z.; Fu, Y.-C.; Yan, J.-W.; Chen, Z.-B.; Mao, B.-W. *Angew. Chem., Int. Ed.* **2009**, *48*, 5148–5151.
(26) Alam, M.; Islam, M.; Okajima, T.; Ohsaka, T. *Electrochem. Commun.* **2007**, *9*, 2370–2374.
(27) Silva, F.; Gomes, C.; Figueiredo, M.; Costa, R.; Martins, A.; Pereira, C. *J. Electroanal. Chem.* **2008**, *622*, 153–160.
(28) Islam, M.; Alam, M.; Okajima, T.; Ohsaka, T. *J. Phys. Chem. C* **2009**, *113*, 3386–3389.
(29) Alam, M.; Islam, M.; Okajima, T.; Ohsaka, T. *J. Phys. Chem. C* **2009**, *113*, 6596–6601.
(30) Bozzini, B.; Bund, A.; Busson, B.; Humbert, C.; Ispas, A.; Mele, C.; Tadjeddine, A. *Electrochem. Commun.* **2010**, *12*, 56–60.
(31) Lockett, V.; Sedev, R.; Ralston, J.; Horne, M.; Rodopoulos, T. *J. Phys. Chem. C* **2008**, *112*, 7486–7495.
(32) Drüschler, M.; Huber, B.; Passerini, S.; Roling, B. *J. Phys. Chem. C* **2010**, *114*, 3614–3617.
(33) Pan, G.-B.; Freyland, W. *Chem. Phys. Lett.* **2006**, *427*, 96–100.
(34) Pan, G.-B.; Freyland, W. *Phys. Chem. Chem. Phys.* **2007**, *9*, 3286–3290.
(35) Freyland, W. *Phys. Chem. Chem. Phys.* **2007**, *10*, 923–936.
(36) Siepmann, J.; Sprik, M. *J. Chem. Phys.* **1995**, *102*, 511–524.
(37) Tang, K.; Toennies, J. *J. Chem. Phys.* **1984**, *80*, 3726–3741.
(38) Heaton, R.; Brookes, R.; Madden, P.; Salanne, M.; Simon, C.; Turq, P. *J. Phys. Chem. B* **2006**, *110*, 11454–11460.
(39) Pounds, M. Ph. D. thesis, University of Edinburgh, 2009.
(40) Salanne, M.; Vuilleumier, R.; Madden, P.; Simon, C.; Turq, P.; Guillot, B. *J. Phys.: Condens. Matter* **2008**, *20*, 494207.
(41) Humphrey, W.; Dalke, A.; Schulten, K. *J. Mol. Graphics* **1996**, *14*, 33–38.
(42) Kislenko, S.; Samoylov, I.; Amirov, R. *Phys. Chem. Chem. Phys.* **2009**, *11*, 5584–5590.
(43) Petit, L.; Vuilleumier, R.; Maldivi, P.; Adamo, C. *J. Phys. Chem. B* **2008**, *112*, 10603–10607.
(44) Baldelli, S. *J. Phys. Chem. B* **2005**, *109*, 13049–13051.
(45) Baldelli, S. *Acc. Chem. Res.* **2008**, *41*, 421–431.
(46) Lynden-Bell, R.; Youngs, T. *J. Phys.: Condens. Matter* **2009**, *21*, 424120.
(47) Borodin, O. *J. Phys. Chem. B* **2009**, *113*, 11463–11478.
(48) Bedrov, D.; Borodin, O.; Li, Z.; Smith, G. *J. Phys. Chem. B* **2010**, *114*, 4984–4997.
(49) O'Sullivan, K.; Madden, P. *J. Phys.: Condens. Matter* **1991**, *3*, 8751–8756.

JP1030448